European Journal of Cell Biology 103 (2024) 151400

Contents lists available at ScienceDirect

European Journal of Cell Biology

journal homepage: www.elsevier.com/locate/ejcb

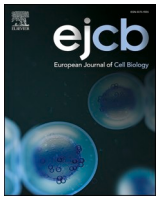

NANOS1 restricts oral cancer cell motility and TGF-ß signaling

Julia Rosemann [a], Jonas Pyko [a], Roland Jacob [a], Jana Macho [a], Matthias Kappler [b], Alexander W. Eckert [c], Monika Haemmerle [d], Tony Gutschner [a,*]

[a] Institute of Molecular Medicine, Section for RNA biology and pathogenesis, Martin Luther University Halle-Wittenberg, Halle 06120, Germany
[b] Department of Oral and Maxillofacial Plastic Surgery, Martin Luther University Halle-Wittenberg, Halle 06120, Germany
[c] Department of Cranio Maxillofacial Surgery, Paracelsus Medical University, Nuremberg 90471, Germany
[d] Institute of Pathology, Section for Experimental Pathology, Martin Luther University Halle-Wittenberg, Halle 06120, Germany

ARTICLE INFO

Keywords:
EMT
HNSCC
Metastasis
OSCC
RNA-binding protein
RBP

ABSTRACT

Oral squamous cell carcinoma (OSCC) is the most frequent type of cancer of the head and neck area accounting for approx. 377,000 new cancer cases every year. The epithelial-to-mesenchymal transition (EMT) program plays an important role in OSCC progression and metastasis therefore contributing to a poor prognosis in patients with advanced disease. Transforming growth factor beta (TGF-ß) is a powerful inducer of EMT thereby increasing cancer cell aggressiveness. Here, we aimed at identifying RNA-binding proteins (RBPs) that affect TGF-ß-induced EMT. To this end we treated oral cancer cells with TGF-ß and identified a total of 643 significantly deregulated protein-coding genes in response to TGF-ß. Of note, 19 genes encoded RBPs with NANOS1 being the most downregulated RBP. Subsequent cellular studies demonstrated a strong inhibitory effect of NANOS1 on migration and invasion of SAS oral cancer cells. Further mechanistic studies revealed an interaction of NANOS1 with the TGF-ß receptor 1 (TGFBR1) mRNA, leading to increased decay of this transcript and a reduced TGFBR1 protein expression, thereby preventing downstream TGF-ß/SMAD signaling. In summary, we identified NANOS1 as negative regulator of TGF-ß signaling in oral cancer cells.

1. Introduction

The transforming growth factor beta (TGF-ß) signaling pathway is an important regulator of multiple cellular processes, including proliferation, apoptosis, stem cell regeneration, immune response and the induction of an epithelial-mesenchymal transition (EMT) program (Principe et al., 2014). EMT normally occurs during embryonic development as well as during fibrosis, wound healing and tissue regeneration. Furthermore, the EMT program is often found to be aberrantly activated during cancer progression and metastasis (Brabletz et al., 2018; Kalluri and Weinberg, 2009). EMT is associated with remodeling of the cellular transcriptome including a decreased expression of E-Cadherin (CDH1) and an enhanced level of N-Cadherin (CDH2), Vimentin (VIM) and other mesenchymal genes, which ultimately leads to the loss of cell-cell contacts and apical-basal polarity as well as a reorganization of the cytoskeleton thereby enhancing the motility of cells. Importantly, the effects of TGF-ß depend on the cellular context, and this contextual nature is particularly manifested in tumors. TGF-ß from the inflammatory tumor microenvironment may cause cancer cell apoptosis and tumor suppression, especially in early stages of carcinogenesis (David and Massague, 2018; Pickup et al., 2013). In contrast, in advanced stages TGF-ß promotes tumor progression by inducing an EMT, which enhances invasion and metastasis and promotes cancer stem cell heterogeneity and drug resistance (Heldin et al., 2012; Oshimori et al., 2015). To initiate signaling, TGF-ß acts through serine/threonine kinase receptors, namely TGFBR1 and TGFBR2 that belong to the type I and type II TGF-ß receptors, respectively. Upon ligand binding, tetrameric TGFBR1/TGFBR2 complexes are formed and activated to transduce downstream signals. In canonical TGF-ß signaling, TGFBR1 phosphorylates receptor-regulated SMADs (R-SMADs), i.e. SMAD2 and SMAD3. Subsequently, cytoplasmic R-SMADs associate with the co-SMAD, SMAD4, to form a trimeric SMAD complex that translocates into the nucleus in order to regulate the transcription of various target genes together with a range of transcription factors and transcriptional modulators (David and Massague, 2018). In the context of TGF-ß-induced EMT several transcription

* Correspondence to: Institute of Molecular Medicine, Section for RNA biology and pathogenesis, Martin Luther University Halle-Wittenberg, Kurt-Mothes-Str. 3a, Halle D-06120, Germany.
E-mail address: tony.gutschner@uk-halle.de (T. Gutschner).

https://doi.org/10.1016/j.ejcb.2024.151400
Received 4 October 2023; Received in revised form 4 February 2024; Accepted 20 February 2024
Available online 21 February 2024

factors, including Snail Family Transcriptional Repressor 1 and 2 (SNAI1/2), Twist and zinc-finger E-box-binding homeobox 1/2 (ZEB1/2), play a critical role by directly regulating the expression of epithelial genes such as E-Cadherin, Plakophilin and Claudins as well as mesenchymal genes such as N-Cadherin, Fibronectin and Collagens (Lamouille et al., 2014). Although these transcriptional changes are important downstream events, TGF-ß signaling also modulates post-transcriptional gene regulatory processes, e.g. mRNA splicing and translation, through the coordinated action of non-coding RNAs and RNA-binding proteins (RBPs) (Howley and Howe, 2019; Janakiraman et al., 2018). In fact, individual RBPs have been established as critical post-transcriptional regulators of EMT and the associated motility phenotype by modulating splicing, stability, localisation or translation of their target RNAs. For example, the epithelial splicing regulatory proteins 1 and 2 (ESRP1/2), which promote an epithelial phenotype, are downregulated upon TGF-ß stimulation and control the alternative splicing of EMT-associated genes such as fibroblast growth factor receptor 2 (FGFR2) (Horiguchi et al., 2012; Warzecha et al., 2010). In contrast, the expression of RNA-binding Fox-1 homolog 2 (RBFOX2), another well-known regulator of alternative splicing, is moderately increased upon TGF-ß-induced EMT and RBFOX2 was shown to regulate EMT-associated splicing in murine mammary epithelial cell lines thereby increasing the invasive potential of these cells (Braeutigam et al., 2014). However, the role of RBFOX2 is controversial as it regulates both, epithelial and mesenchymal splicing events (Baraniak et al., 2006; Venables et al., 2013). In line with this, a recent study suggests a role of RBFOX2 as a potent metastasis suppressor in pancreatic ductal adenocarcinoma (PDAC) (Jbara et al., 2023). Additional RBPs that regulate the epithelial or mesenchymal phenotype have been identified in the past decade and several of these proteins belong to the heterogeneous nuclear ribonucleoprotein (hnRNP) family. For example, the ubiquitously expressed hnRNP M acts in a mesenchymal-specific manner to control cluster of differentiation 44 (CD44) isoform switching during EMT. Moreover, depletion of hnRNP M prevents TGF-ß-induced EMT and inhibits breast cancer metastasis in mice (Xu et al., 2014). Similarly, hnRNP A/B binds to the SNAI1 promoter, which activates gene transcription and promotes EMT and metastatic progression of human hepatocellular carcinoma (HCC) (Zhou et al., 2014). In contrast, hnRNP A1 prevents EMT and instead activates the reverse program, namely the mesenchymal-to-epithelial transition (MET) by inhibiting alternative splicing of the Macrophage Stimulating 1 Receptor (MST1R), a tyrosine kinase receptor also known as RON (Bonomi et al., 2013). Last but not least, hnRNP E1, also known as Poly(rC)-Binding Protein 1 (PCBP1), has been shown to acts as a tumor suppressor in several cancer types by regulating the epithelial phenotype. Consequently, silencing of hnRNP E1 induces EMT, increases cell motility, and promotes tumor formation and distant metastases (Chaudhury et al., 2010; Hussey et al., 2011; Tripathi et al., 2016; Wang et al., 2010; Zhang et al., 2016, 2015). Interestingly, hnRNP E1 is a multi-functional downstream effector of TGF-ß signaling that regulates its target transcripts through diverse mechanisms, including alternative splicing, translational repression, and control of alternative polyadenylation (Howley and Howe, 2019).

While these examples highlight the importance of post-transcriptional gene regulation by RBPs in the context of TGF-ß-induced EMT, further research is needed in order to fully understand the role of RBPs as downstream targets and modulators of the TGF-ß signaling pathway. In this study, we analyzed the invasion-promoting effect of TGF-ß on human oral cancer cells. We observed increased invasion of SAS cells upon cytokine stimulation and performed RNA-sequencing in order to map transcriptome-wide gene expression changes. In addition to the expected EMT-related alterations, we identified a set of RBPs whose expression was significantly modulated, with NANOS1 representing the most downregulated RBP in TGF-ß-treated SAS cells. Intriguingly, forced overexpression of NANOS1 completely blocked the cellular response to TGF-ß suggesting that the observed downregulation of NANOS1 is necessary for a robust pathway activation. Mechanistically, NANOS1, a well-known regulator of RNA stability, associated with TGFBR1 mRNA leading to its destabilization. Consequently, NANOS1 overexpressing cells showed a reduced TGFBR1 protein expression and thus became incapable of sensing and responding to TGF-ß. Hence, we discovered a novel function of NANOS1 acting as a post-transcriptional, negative regulator of oncogenic TGF-ß signaling.

2. Materials and methods

2.1. Cell lines and cell culture including TGF-ß stimulation

The human squamous cell carcinoma cell lines FaDu (hypopharynx), Cal33 (oral tongue), XF354 (oral cavity) and SAS (oral tongue), kindly received from Prof. Daniel Zips, were cultured in RPMI-1640 medium containing 10% Fetal bovine serum (FBS), 100 U/mL Penicillin, 100 µg/mL Streptomycin (all from Thermo Fisher Scientific, Waltham) and supplemented with 1% sodium pyruvate (Sigma-Aldrich, St. Louis) at 37 °C and 5% CO_2. HEK293T cells (ACC 635, DSMZ, Braunschweig) for production of lentiviral particles and A-375 melanoma cells (CRL-1619, ATCC, Manassas) were cultured in DMEM (Thermo Fisher Scientific) supplemented with 10% FBS. Cells were regularly tested for contamination with mycoplasma. To analyze the effects of TGF-ß, cells were treated with 10 ng/mL TGF-ß1 (PreproTech, Cranbury).

2.2. Cloning

A modified pCW-Cas9 plasmid (a gift from Eric Lander & David Sabatini, Addgene plasmid # 50661; (Wang et al., 2014)), which allows Doxycycline-inducible expression of the vector-encoded transgene was generated by replacing Cas9 with a N-terminal FLAG/HA-tag followed by a multiple cloning site (MCS). A gBlock fragment containing a codon-optimized open reading frame of the human NANOS1 gene with a reduced GC-content was synthesized by Integrated DNA Technologies (IDT, Coralville). The gBlock was digested with *Nhe*I and *Xho*I (Thermo Fisher Scientific) and cloned in two consecutive rounds into the respective MCS of the modified pCW-vector to allow expression of FLAG/HA-NANOS1.

2.3. Lentiviral transduction and NANOS1 overexpression

The pCW-FLAG/HA-NANOS1 or pCW-FLAG/HA-MCS (empty vector, EV) plasmids were transfected into HEK293T cells along with the packaging vector psPAX2 and the envelope expressing vector pMD2.G (gifts from Didier Trono, Addgene plasmids #12260 and #12259, respectively) using Turbofect (Thermo Fisher Scientific) according to the manufacturer's instructions. Lentiviral particles were collected after 72 h and filtered through a 0.45 µm membrane (TPP, Trasadingen). For transduction, cells were mixed with fresh lentiviral stocks and allowed to attach. For subsequent antibiotic selection of transduced cells, puromycin (1.5 µg/mL; Thermo Fisher Scientific) was added that resulted in complete cell death of non-transduced control cells within 48 – 72 hours. NANOS1 expression in stably transduced cells was induced by addition of 1 µg/mL Doxycycline (Sigma-Aldrich).

2.4. Transfection of small interfering RNA (siRNA)

For siRNA transfection, 1.25 pmol siRNA and 6 µL transfection reagent (RNAiMax, Thermo Fisher Scientific) were mixed with 200 µL Opti-MEM (Thermo Fisher Scientific) medium and incubated for 15 min at room temperature in an empty 6-well cavity. 6×10^5 cells were added dropwise to the pre-incubated transfection mix. The following siRNAs targeting were applied: siNANOS1_1 (5′-GGAACAA-CAAGGAGGCGAUdTdT-3′) and siNANOS1_2 (5′-GGAAAGCACAAU-GUUUCUUdTdT-3′). As non-targeting siRNA control (siCon), siAllStars Negative Control siRNA (Qiagen, Hilden) was used.

2.5. Wound healing assay

To analyze 2D cell migration, 5.5 $\times 10^4$ cells in 100 µL cell culture medium were seeded in a well of a 96-well plate. The cells were allowed to settle and attach for 16 h at 37 °C and 5% CO_2. A wound through the cell monolayer was created using the IncuCyte 96-well woundmaker tool (Essen Bioscience, Goettingen). After washing the cells, 100 µL cell culture medium was added and pictures were taken every 2 h during a 24 h period. The wound width was calculated using the IncuCyte software. The relative wound density or the time until the moving front of cells migrated 500 nm was calculated using GraphPad Prism software 8.0 (GraphPad Software, San Diego).

2.6. Invasion assay

Analysis of 3D-matrigel invasion was performed as described previously (Weiße et al., 2021). Briefly, 1 $\times 10^3$ cells in 50 µL cell culture medium were seeded in an ultra-low-attachment round bottom 96-well plate (Corning, New York), centrifuged at 300 g for 6 min and incubated at 37 °C and 5% CO_2. After 16 h, 50 µL matrigel (Corning) was added at 4 °C and the cells centrifuged again at 4 °C, 300 g for 6 min. Solidification of the matrigel was achieved by incubation of the spheres for 30 min at 37 °C. Pictures were taken immediately after this incubation and afterwards every 6 h during a 48 h period using an IncuCyte S3 (Essen Bioscience).

2.7. Boyden chamber assay

In order to study trans-migration or trans-invasion of tumor cells, transwell inserts (ThinCerts™, Greiner, Kremsmünster) with a pore size of 8.0 µm were either used uncoated (migration), or coated (invasion) using a mixture of laminin (50 µg/mL, Sigma-Aldrich), collagen IV (1 mg/mL) and gelatin (5 mg/mL) resolved in PBS and incubated while shaking at room temperature for 2 h. The matrix was removed and the membranes air-dried for 30 min under the laminar flow hood. Subsequently, 7.5 $\times 10^4$ cells in 100 µL cell culture medium without FBS were seeded into the upper chamber. The inserts were put into a well of a 24-well plate containing 500 µL complete cell culture medium (10% FBS). After a 16 h incubation period the cells on the lower side of the membrane were fixed with 200 µL methanol at −20 °C for 15 min and subsequently stained for 20 min using Giemsa solution (Carl Roth, Karlsruhe). The inserts were dried for 24 h at room temperature and covered on glass slides. For quantification five pictures were taken and the proportion of the colored and total membrane fractions was measured using Fiji ImageJ 1.52i software (Schneider et al., 2012).

2.8. RNA isolation and quantitative real-time polymerase chain reaction (qRT-PCR)

For RNA isolation 2 $\times 10^5$ cells were seeded in 6-well plates and cells were harvested 48 h later using 1 mL TRIZOL as described previously (Dorn et al., 2020). Total RNA was resuspended in 20 µL ultrapure water (Life Technologies, Carlsbad) and 2 µg were reverse transcribed into cDNA using random hexamers and M-MLV Reverse Transcriptase (Promega, Madison). PCR was performed using primaQuant CYBR-qPCR-Mastermix (Steinbrenner, Wiesenbach) on a Light Cycler I (Roche, Basel). *RPLP0* and *PPIA* were used as reference genes. Sequence information for primers used in qRT-PCR can be found in Table 1 below:

Table 1
List of RT-qPCR primers used in this study.

Gene	primer direction	primer sequence (5' > 3')
AFF3	forward	CAGTGCCGATTATTTTATGCAA
AFF3	reverse	TGCATTTCCACACTCGATAAAC
CDH1	forward	CGGGAATGCAGTTGAGGATC
CDH1	reverse	AGGATGGTGTAAGCGATGGC
CDH2	forward	AAGTGGCAAGTGGCAGTAAAAT
CDH2	reverse	CCAGTCTCTCTTCTGCCTTTGT
CELF2	forward	CACTCAGACCAACCAGACCC
CELF2	reverse	AGTGCATTCTGGGCCTCAAG
GAPDH	forward	CTGGTAAAGTGGATATTGTTGCCAT
GAPDH	reverse	TGGAATCATATTGGAACATGTAAACC
MEX3B	forward	AGTACCCAGTTCTGAGCATGTC
MEX3B	reverse	TGAGTGCCGTGTTCTTATTCCG
NANOS1	forward	TCCCCATTTGTCTTCAGTTTCT
NANOS1	reverse	ATAAACAGCGCCTCTAAGTTGC
PPIA	forward	GTCAACCCCACCGTGTTCTT
PPIA	reverse	CTGCTGTCTTTGGGACCTTGT
RNU6	forward	CTCGCTTCGGCAGCACA
RNU6	reverse	AACGCTTCACGAATTTGCGT
RPLP0	forward	GGCGACCTGGAAGTCCAACT
RPLP0	reverse	CCATCAGCACCACAGCCTTC
TGFBR1	forward	GTTCCGTGAGGCAGAGATTTAT
TGFBR1	reverse	CCGTGGACAGAGCAAGTTTTA
VIM	forward	ATGCGTGAAATGGAAGAGAACT
VIM	reverse	TGTAGGTGGCAATCTCAATGTC

2.9. mRNA-sequencing and gene expression analysis

For mRNA-sequencing, 2 µg of total RNA per sample were used. PolyA-based library preparation and sequencing was performed by Genewiz (Leipzig). Sequencing was performed with approximately 20 million reads per sample using an Illumina NovaSeq platform. Trim Galore! v0.4.3.1 was used for quality check (80% bases Q $\geq$ 30). Mapping to the human genome hg38 followed by differential gene expression analysis was performed using RNA STAR v2.6.0b-2 and edgeR v 3.24.1. Heatmaps with hierarchical clustering have been created in RStudio/2023.09.0+463, (R version 4.3.1), using the R package gplots (v 3.1.3; https://CRAN.R-project.org/package=gplots).

2.10. Gene set enrichment analysis

Differentially expressed protein-coding genes were pre-ranked according to their Log2 fold change and analyzed using the GSEA software (Mootha et al., 2003; Subramanian et al., 2005). The enrichment statistics were calculated using the 'classic' method settings. Results with a FDR q-value $\leq$ 0.05 were considered statistically significant.

2.11. RNA stability analysis

For the analysis of RNA stability, 1 $\times 10^5$ cells in 2 mL cell culture medium were seeded in a 6-well plate and incubated for 48 h in Doxycycline-containing medium. The medium was replaced by fresh medium containing 10 µM α-amanitin (A. Hartenstein, Wuerzburg). The cells were harvested after different incubation periods with 1 mL TRIZOL, total RNA was isolated and RT-qPCR was performed. The expression of RNU6 was used for normalization.

2.12. RNA immunoprecipitation (RIP)

To purify protein-RNA complexes, 4 $\times 10^6$ cells were seeded into 15 cm dishes and incubated for 48 h. Before harvesting, ANTI-FLAG® M2 Affinity Gel agarose beads (Sigma-Aldrich) were blocked overnight in 1 mL blocking buffer (20 µg/mL tRNA (Roche, Basel), 20 µg/mL Glycogen (Serva, Heidelberg), 10 µg/µL Bovine Serum Albumin (BSA; AppliChem, Darmstadt) ad 1 mL lysis buffer (62.5 mM Tris-HCl pH8.0, 187.5 mM NaCl, 1.25% (v/v) IGEPAL CA-630, 0.625% (v/v) Na-deoxycholate, 0.125% (w/v) SDS). Meanwhile, cells were washed three times with ice cold PBS (Thermo Fisher Scientific) and harvested using Rotilabo®-rubber wipers (Carl Roth). The cell pellet was resuspended in 800 µL lysis buffer and incubated on ice. After complete removal of the blocking buffer from the pre-incubated beads, approximately 75% of the cell lysate was added to the blocked anti-FLAG beads followed by an incubation at 4 °C for 2.5 hours under gentle rotation. A fraction of the initial cell lysate was used for RNA isolation ('RNA Input')

and another for western blotting ('protein input'). Finally, beads were washed three times with 1X TBS-T (10X TBS: 247 mM Tris Base, 1.37 M NaCl, 26.8 mM KCl; 1:1000 Tween20 (Sigma-Aldrich)). For analysis of NANOS1-RNA interactions, approximately 80% of beads were resuspended in TRIZOL for RNA isolation and 20% were resuspended in protein sample buffer for western blot analysis.

2.13. Western blotting

Cells were harvested followed by the lysis of the pellet using RIPA lysis buffer (50 mM Tris-HCl pH 8.0, 150 mM NaCl, 1% (v/v) IGEPAL CA-630, 0.5% (w/v) Na-deoxycholate, 0.1% (w/v) SDS) supplemented with protease and phosphatase inhibitors (Roche, Basel). SDS-Polyacrylamid gel electrophoresis (SDS-PAGE) was performed for 1–2 hours at 120 V depending on the acrylamide concentration of the resolving gel (8–12%). The wet blot method was used to transfer proteins onto a nitrocellulose membrane (Th.Geyer, Renningen). Protein expression levels were evaluated using Odyssey infrared scanner (LI-COR, Lincoln). The following primary antibodies were used: ACTB (clone AC-15, Sigma-Aldrich), CDH1 (#3195), CDH2 (#14215), VIM (#5741), SMAD2 (#5339), SMAD3 (#9523), P(S465/467)-SMAD2 (#3108), P(S423/425)-SMAD3 (#9520, all from Cell Signaling Technology, Danvers), RPL7 (#A300–741A), TGFBR1 (#PA5–98192, all from Thermo Fisher Scientific, Waltham), and NANOS1 (#TA344042, OriGene Technologies, Rockville; #PA5-18356, Invitrogen, Waltham). The following secondary antibodies were used respectively: IRDye® 800CW Donkey anti-Rabbit, IRDye® 680RD Donkey anti-Rabbit, IRDye® 800CW Donkey anti-Goat, IRDye® 680RD Donkey anti-Mouse (all from LI-COR).

2.14. Immunofluorescence

5 $\times 10^4$ cells were seeded on coverslips and cultured for 48 h. After incubation, the cells were washed and fixed for 30 min using paraformaldehyde (Carl Roth, Karlsruhe) followed by the treatment with 0.5% (w/v) Triton-X-100 (Carl Roth) in PBS (Thermo Fisher Scientific). The cells were blocked in 1% (w/v) BSA (AppliChem) in PBS followed by overnight incubation at 4 °C using the following primary antibodies diluted 1:200 in 1% (w/v) BSA/PBS: E-Cadherin (#3195), Vimentin (#5741) or Smad2/3 (#8685, all Cell Signaling). Afterwards, the slides were washed twice with PBS and then incubated for 1 h with a secondary α-rabbit AlexaFluor® 488 antibody (Jackson ImmunoResearch Laboratories, Baltimore). Nuclei were stained with DAPI (1 μg/mL; Carl Roth) and the coverslips were mounted using Mowiol (Calbiochem, San Diego). Pictures were taken using a confocal microscope (Leica SP8X, Leica, Wetzlar) and Leica LAS AF software. The ImageJ software (Schindelin et al., 2012) was used for image analysis.

2.15. TGF-β/SMAD signaling luciferase reporter assay

TGF-ß/SMAD signaling was investigated performing Luciferase reporter assay using the Nano-Glo Dual-Luciferase Reporter Assay System (Promega, Madison). For plasmid transfection, SAS cells overexpressing NANOS1 or empty vector were seeded in 24-well cell culture plate (Corning) and transfected 24 h after seeding with a SMAD3/SMAD4 binding element (SBE) reporter plasmid (pNL[NlucP/SBE/Hygro]) driving NanoLuc expression in response to TGF-ß. For transfection control, pGL4.54 [luc2/TK] (Vector GenBank Accession Number KM359769) expressing thymidine kinase promoter-driven firefly luciferase was co-transfected. Cells were treated with 10 ng/mL TGF-ß1 (PeproTech) 24 h after transfection and luminescence was measured 48 h post-transfection. Reactions were performed in technical triplicates using a white 96-well microplate (LUMITRAC™200, Greiner). Luminescence signals were measured using an Infinite 200 PRO microplate reader (Tecan, Männedorf). The luminescence signal of NanoLuc (NL) was divided by the firefly luciferase (FF) signal for normalization.

2.16. Correlation of NANOS1 expression with clinical data

NANOS1 association with patient survival and molecular subtypes in head and neck squamous cell carcinoma (HNSCC) and skin cutaneous melanoma (SKCM) was retrieved from the GEPIA2 portal (Tang et al., 2019). Its association with overall patient survival in tumors of different anatomic sites was revealed using R2: Genomics Analysis and Visualization Platform (http://r2.amc.nl).

2.17. Statistical analysis

All experiments presented in this work were carried out at least in three biologically independent experiments. The exact number of each experiment is indicated in the respective figure legend. Mean values and standard deviations were calculated and the comparison of two groups was analyzed using unpaired two-tailed Student's t-test. Ordinary one-way ANOVA was used for multiple comparisons and for grouped results two-way ANOVA was performed. Differences were considered significant when $p \leq 0.05$ (*$p \leq 0.05$; **$p \leq 0.01$; ***$p \leq 0.001$; ****$p \leq 0.0001$).

3. Results

3.1. TGF-β selectively enhances the invasion capacity of head and neck squamous cell carcinoma-derived cancer cells

In order to investigate the invasion-promoting effect of TGF-ß, we initially treated a panel of four human head and neck squamous cell carcinoma (HNSCC) cell lines with TGF-ß and followed their invasive growth in a three-dimensional (3D) matrigel-based invasion assay. While TGF-ß was not able to stimulate the motility of non-invasive Cal33, XF354 and FaDu cells (Suppl. Fig. 1), the motility of highly invasive SAS cells was even further enhanced upon TGF-ß treatment. In detail, we observed an approximately 4-fold increase in 3D matrigel invasion (Fig. 1A) as well as a ~1.5-fold higher trans-migration rate (Fig. 1B) of TGF-ß treated SAS cells compared to non-treated control cells. Since TGF-ß is known to promote cancer cell invasion by inducing EMT, we analyzed the expression of established epithelial and mesenchymal markers using RT-qPCR and western blotting in SAS cells (Fig. 1C, D). We were able to confirm a reduction of CDH1 mRNA and protein upon TGF-ß stimulation. Moreover, TGF-ß treated SAS cells strongly up-regulated the transcript levels of the mesenchymal genes CDH2 and VIM, which led to a more than 2-fold increase in the abundance of the respective proteins. Taken together, our initial analyses revealed a cell type-dependent capacity to invade a 3D matrigel-based matrix under normal growth conditions and demonstrated an EMT and invasion-promoting effect of TGF-ß signaling in SAS oral cancer cells.

3.2. TGF-β regulates the expression of RNA-binding proteins in SAS cells

Next, we wanted to obtain deeper insights into TGF-ß-induced gene expression changes in oral cancer cells. Specifically, we were interested in identifying RBPs whose expression would be modulated by TGF-ß in SAS cells. Therefore, we stimulated the cells for 48 hours with 10 ng/mL TGF-ß1, isolated total RNA and performed mRNA-sequencing. Comparison of the expression pattern between treated and non-treated cells identified a total of 976 significantly (FDR ≤ 0.05) deregulated protein-coding genes of which 535 showed an increased and 441 a decreased expression upon TGF-ß treatment (Fig. 2A, B and Supplementary Data 1). Setting a log2 fold change (log2FC) cut-off at $|\log2FC| \geq 1$ reduced this list to 643 significantly altered protein-coding genes (344 up- and 299 down-regulated). Performing gene set enrichment analysis (GSEA) allowed us to identify pathways associated with TGF-ß stimulation in SAS cells. As expected, the "Hallmark" gene sets EPITHELIAL_MESENCHYMAL_TRANSITION (EMT) and

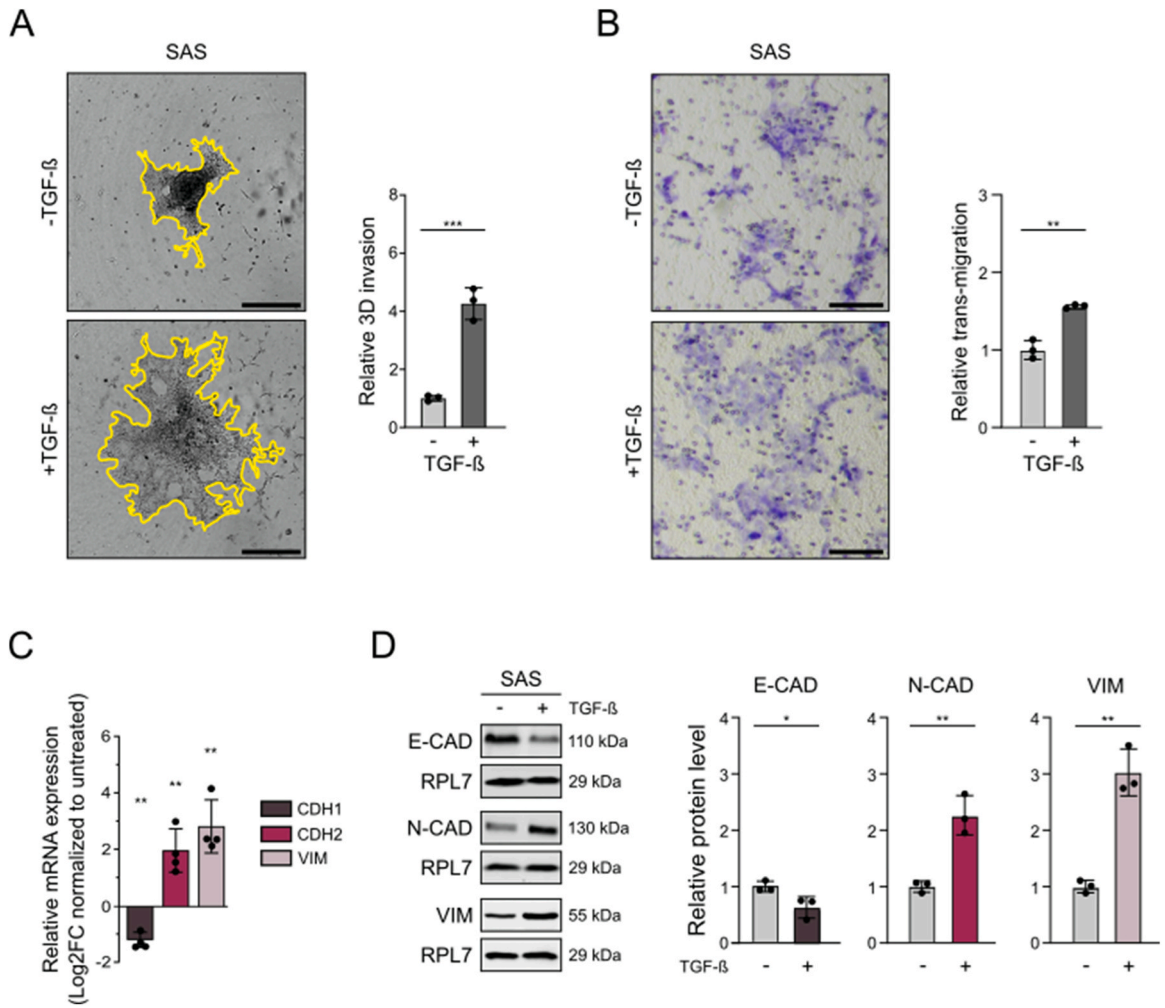

Fig. 1. TGF-ß increases SAS cell motility and induces EMT. A) 3D-matrigel invasion assays were performed using SAS oral cancer cells treated with 10 ng/mL TGF-ß1. Representative images and quantification of three independent biological replicates are shown. Pictures were taken after 24 h. The invasive front is marked in yellow (scale bar = 400 µm). B) Boyden chamber trans-migration assays were performed for 16 h with SAS treated with 10 ng/mL TGF-ß1 (48 h) or without cytokine stimulation. Representative images and quantification of the relative migration rate in three independent biological replicates are shown. C) RT-qPCR analysis showing mRNA abundance changes in E-Cadherin (CDH1), N-Cadherin (CDH2) and Vimentin (VIM) after treatment of SAS cells with 10 ng/mL TGF-ß1 for 48 h. Expression changes relative to untreated cells are displayed. Normalization was performed using RPLP0 and PPIA. D) Western blot analysis of SAS treated with TGF-ß1 for 48 h to detect E-Cadherin, N-Cadherin and Vimentin. RPL7 served as loading control. Representative blots on the left and quantification of three independent biological replicates on the right.

TGF_BETA_SIGNALING had a positive normalized enrichment score (NES), whereas cell cycle-related gene sets had a negative NES. All 32 enriched gene sets with a FDR q-value ≤ 0.05 are shown in Fig. 2C. This unbiased analysis confirmed the known impact of TGF-ß on gene expression and cellular behavior and validated our treatment protocol.

To ultimately identify TGF-ß-regulated RBPs we intersected our list of 976 significantly deregulated protein-coding genes with a list of 1542 human RBPs that had previously been included in a manually curated RBP census (Gerstberger et al., 2014). This intersection revealed a total of 19 RBPs, which were significantly deregulated by TGF-ß in SAS cells (Fig. 2D). Two RBPs, namely AFF3 and MEX3B, showed a more than 2-fold increase whereas another seven RBPs (OASL, RBM47, PEG10, IFIT2, IFIT3, CELF2 and NANOS1) were reduced by more than 2-fold at the transcript level (Fig. 2E). We selected the top four differentially regulated RBPs and validated the expression changes upon TGF-ß treatment using RT-qPCR (Fig. 2F). From this selection of RBPs NANOS1 caught our attention, as it was previously shown to promote breast, colon and lung cancer cell motility and to be negatively regulated by E-Cadherin (Bonnomet et al., 2008; Strumane et al., 2006). However, in our oral cancer cell system NANOS1 was strongly downregulated at the RNA and protein level after the induction of an EMT (Fig. 2G). This observation suggested a novel, potentially inhibitory function of this well-known RBP in the context of TGF-ß signaling in oral cancer cells.

3.3. NANOS1 inhibits migration and invasion of SAS cells and restricts TGF-ß effects

To characterize the cellular function of NANOS1 in detail we performed gain- and loss-of-function analyses. First, we transiently depleted NANOS1 in SAS cells using two independent siRNAs (Suppl. Fig. 2). Intriguingly, the knockdown of NANOS1 increased the trans-migration of SAS cells about 2-fold (Fig. 3A). Next, we cloned an optimized coding sequence of human NANOS1 in frame with a N-terminal FLAG/HA-tag into a lentiviral vector that contained a Doxycycline-inducible promoter. After infection of SAS cells with the corresponding lentivirus we added Doxycycline and observed an efficient induction of NANOS1 protein (Fig. 3B). In parallel, we also generated SAS cells that integrated an empty vector (EV) and served as controls in subsequent assays. In order to investigate the cellular effects of NANOS1 overexpression, we initially analyzed 2D migration of SAS cells in a wound healing assay

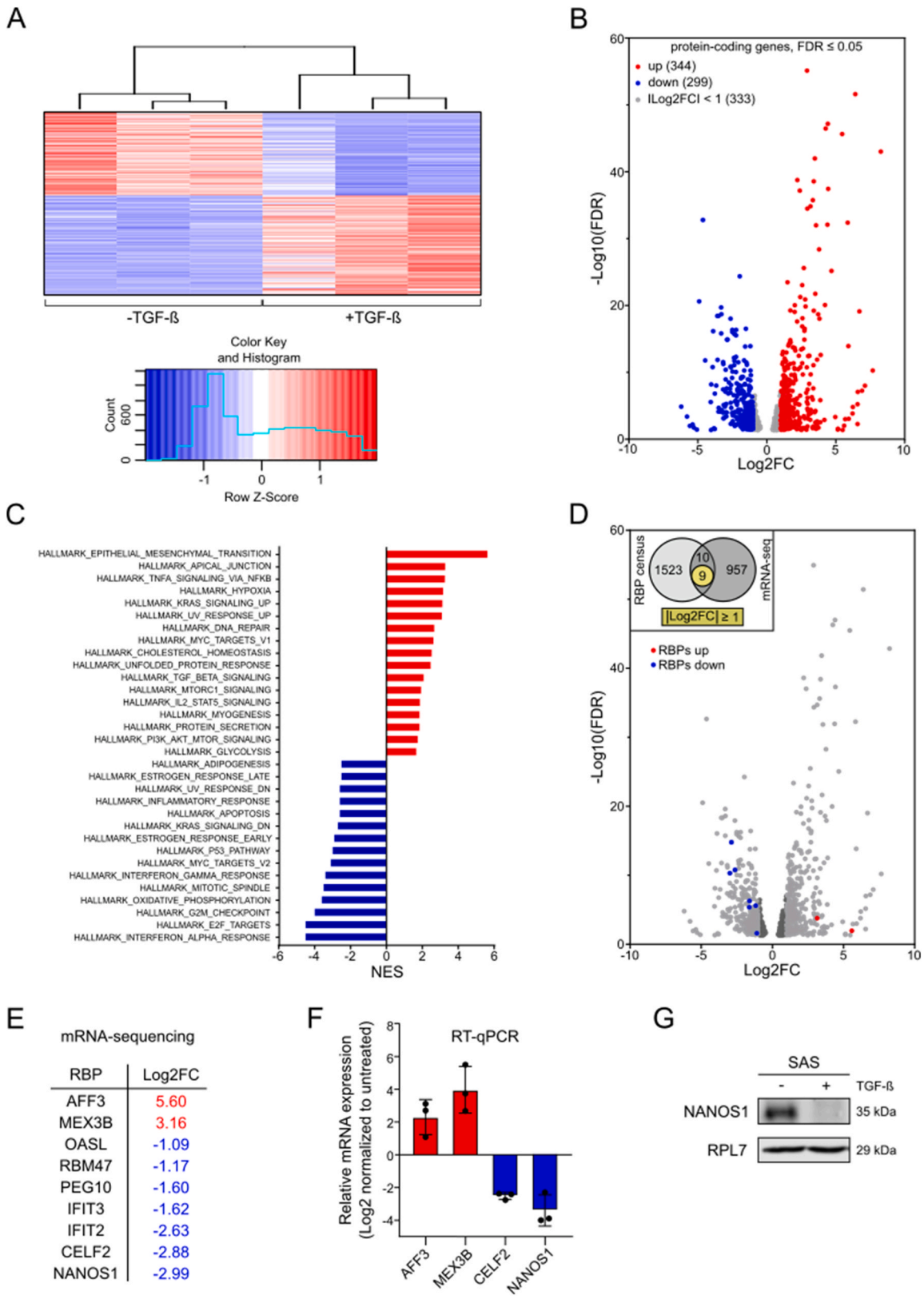

Fig. 2. TGF-ß alters the expression of RNA-binding proteins in SAS cells. A) Heatmap of significantly differentially expressed genes (FDR $\leq$ 0.05) after TGF-ß1 stimulation (48 h). B) Volcano plot of 976 differentially expressed protein-coding genes with FDR $\leq$ 0.05. C) GSEA analysis of mRNA-sequencing data considering all protein-coding genes revealed a significant enrichment of 17 as well as a reduction of 15 gene sets upon TGF-ß1 treatment. D) Same volcano plot as in A) with individual data for RNA-binding proteins showing a $|Log2FC| \geq 1$ being highlighted in red (2 upregulated RPBs) and blue (7 downregulated RBPs). E) List of selected significantly altered RBPs and their respective Log2FC values from mRNA-Seq. F) Independent validation of TGF-ß-induced mRNA expression changes of four selected RBPs relative to untreated SAS cells using RT-qPCR (n = 3). Normalization was performed using RPLP0 and PPIA. G) Representative western blot confirming the downregulation of NANOS1 protein expression after TGF-ß1 stimulation in SAS cells. RPL7 served as loading control.

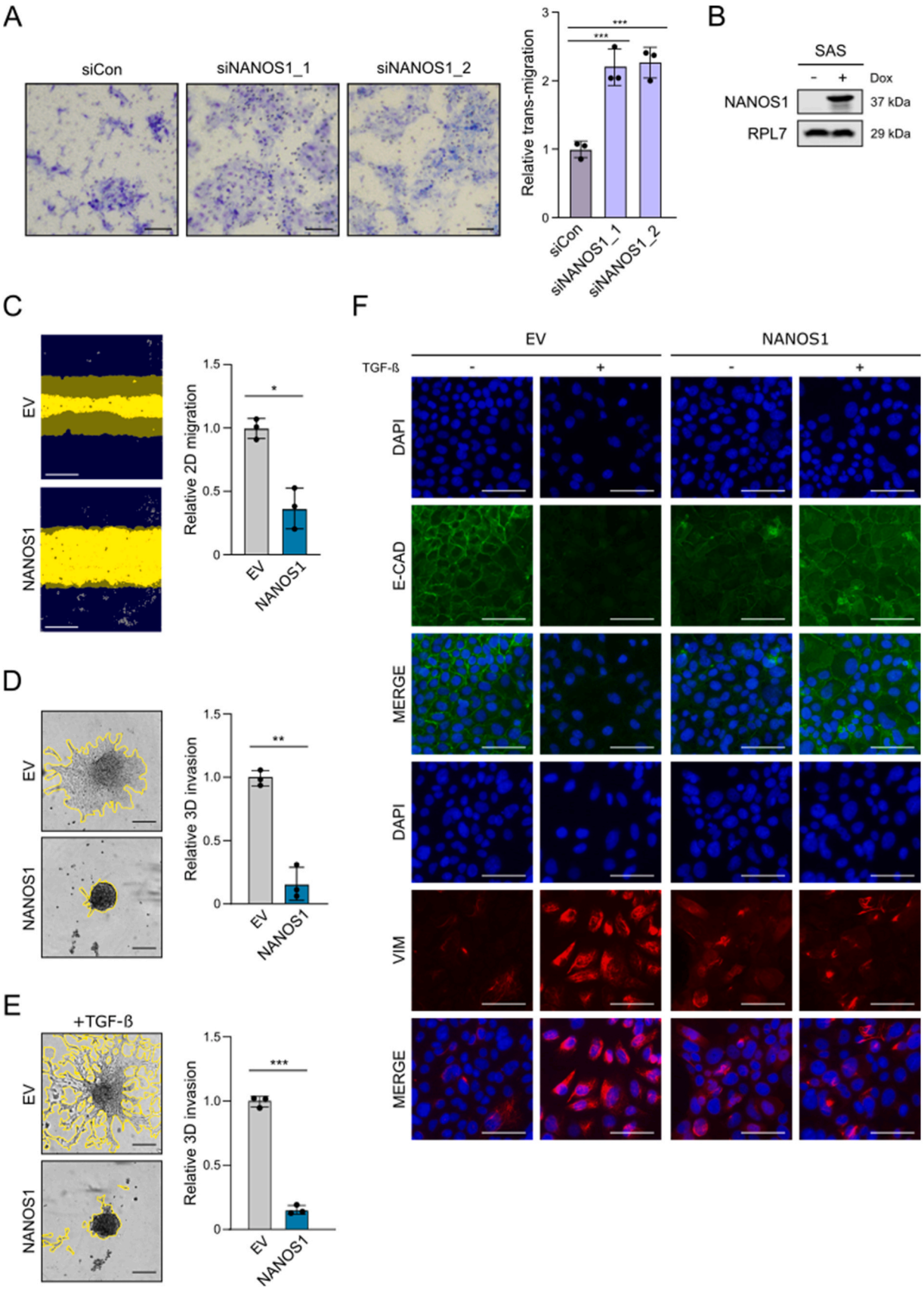

(caption on next page)

Fig. 3. NANOS1 limits cell motility and prevents a cellular response to TGF-ß. A) Boyden chamber trans-migration assays in SAS cells after transient depletion of NANOS1 using two independent siRNAs. Cells were seeded on membranes 32 h after transfection of siRNAs and relative trans-migration (normalized to siControl) was analyzed 16 h later. Representative pictures of membranes and quantification of three independent biological replicates are shown. B) Representative western blot showing the Doxycycline-dependent overexpression of FLAG/HA-tagged NANOS1. RPL7 served as loading control. C) Wound healing assay to analyze 2D migration of SAS cells overexpressing NANOS1 or EV control both treated 48 h with 1 μg/mL Doxycycline. Images taken every 2 h for a period of 24 h. Displayed are representative pictures 8 h after the scratch wound was initiated. yellow – initial scratch wound, dark blue – cells, grayish – moving cells closing the wound. Scale bar 400 μm. Quantitative analysis of relative migration (mean of EV set to 1.0, n = 3) is shown. D) 3D matrigel invasion assay with SAS overexpressing NANOS1 or EV. The cells were treated for 48 h with 1 μg/mL Doxycycline prior to the addition of matrigel. Shown are representative images taken 12 h after adding matrigel. The invasive front of the cells is colored in yellow. Quantitative analysis of relative invasion (mean of EV set to 1.0, n = 3) is shown. E) Analysis of 3D matrigel invasion after TGF-ß1 stimulation. Analysis done as in D). F) NANOS1 and EV control cells were treated for 48 h with 1 μg/mL Doxycycline and 10 ng/mL TGF-ß1 was added or not. Representative images of two independent biological experiments show E-Cadherin (green) and Vimentin (red) expression and localization. Nuclei are stained with DAPI (blue).

and observed a strong and significant inhibitory effect of NANOS1 (Fig. 3C). Furthermore, NANOS1 overexpression strongly impaired the 3D invasion of transgenic cells as assessed by a matrigel-based invasion assay (Fig. 3D). Motivated by these findings and the fact that NANOS1 was downregulated upon TGF-ß stimulation, we asked whether forced expression of NANOS1 could affect the cellular response to TGF-ß. Hence, we treated SAS control cells (EV) and NANOS1 overexpressing cells with the cytokine and analyzed the invasiveness of the cells. Surprisingly, while control cells showed the expected increase in their invasiveness, NANOS1 overexpression strongly restricted the pro-invasive effect of TGF-ß (Fig. 3E). To test if this reduced motility, especially after TGF-ß stimulation, might be due to a differential regulation of cell adhesion and cytoskeletal proteins we performed immunofluorescence analyses. We stained for E-Cadherin and Vimentin and observed the expected down-regulation of E-Cadherin and up-regulation of Vimentin indicative of an EMT in TGF-ß-treated control (EV) cells (Fig. 3F). Remarkably, TGF-ß was not able to modulate E-Cadherin and Vimentin expression and to induce an EMT in NANOS1 overexpressing cells. This observation is well in line with the restricted TGF-ß response seen in the invasion assay (Fig. 3E). In conclusion, NANOS1 inhibits the invasion and migration of SAS cells and seems to interfere with the pro-invasive effects of TGF-ß signaling.

3.4. Overexpression of NANOS1 affects the expression of TGF-β pathway genes

To better understand how the RNA-binding protein NANOS1 is able to affect cell motility and TGF-ß signaling we performed mRNA-sequencing after induction of NANOS1 expression. In detail, overexpression of NANOS1 in SAS cells significantly modulated the expression of 5088 genes (2509 up and 2579 down; FDR $\leq$ 0.05). Further filtering for genes whose expression was altered by at least 2-fold left 1361 up-regulated and 1186 down-regulated genes (Fig. 4A, B and Supplementary Data 2). Next, we performed a GSEA analysis to identify gene sets or pathways influenced by NANOS1. This analysis revealed a total of 42 differentially enriched "Hallmark" gene sets with a FDR q-value $\leq$ 0.05 (Fig. 4C). Of note, the "Hallmark" gene sets EPITHELIAL_MESENCHYMAL_TRANSITION (EMT) and, in particular, TGF_BETA_SIGNALING showed a strong negative NES suggesting a repression of genes associated with the TGF-ß pathway (Fig. 4D). In fact, 26 out of 54 genes that belong to the HALLMARK_TGF_BETA_SIGNALING gene set were significantly (FDR $\leq$ 0.05) deregulated with 24 out of these 26 genes showing a decreased expression in NANOS1 overexpressing cells (Fig. 4E). Interestingly, we noted that the TGFBR1 mRNA was strongly (Log2FC = −1.95) reduced.

3.5. NANOS1 regulates TGFBR1 abundance and impairs downstream signaling

In order to test whether NANOS1 could directly regulate TGFBR1 expression and thereby affecting the signal transduction capabilities and responsiveness of the cells, we initially validated the decreased TGFBR1 abundance upon NANOS1 overexpression, both at the transcript as well as the protein level. Indeed, we observed nearly a 70% reduction at the mRNA level (Fig. 5A) and approximately 60% reduction of the TGFBR1 protein upon NANOS1 overexpression (Fig. 5B). On the other hand, knockdown of NANOS1 increased TGFBR1 mRNA abundance by nearly 50% (Fig. 5C). Next, we investigated whether the NANOS1-dependent reduction of TGFBR1 expression was correlated with a direct association of NANOS1 with the TGFBR1 mRNA. Therefore, we performed RNA immunoprecipitation (RIP) experiments. We treated transgenic SAS cells with Doxycycline to induce the expression of FLAG/HA-tagged NANOS1. Subsequently, we purified the RBP using anti-FLAG affinity beads. Non-induced cells, i.e. cells that did not express the tagged NANOS1 protein served as negative control. After we verified a specific pull-down of NANOS1 (Fig. 5D) we isolated the co-purified RNA and analyzed the enrichment of selected transcripts using RT-qPCR. This analysis revealed a specific enrichment of the TGFBR1 mRNA in NANOS1-IPs and a 3-fold higher binding affinity of NANOS1 to TGFBR1 mRNA compared to GAPDH mRNA (Fig. 5**E**). Since NANOS1 is known to destabilize its target RNAs (De Keuckelaere et al., 2018; Ilaslan et al., 2022), we tested whether its overexpression would reduce TGFBR1 mRNA stability. To this end EV control and NANOS1 overexpressing SAS cells were treated for 24 h with α-amanitin to preferentially inhibit RNA polymerase II-dependent transcription. We isolated total RNA, performed RT-qPCR and analyzed the change in the TGFBR1 transcript abundance. Intriguingly, while EV control cells still contained ~34% of the initial TGFBR1 mRNA amount after 24 h, NANOS1 overexpression led to an enhanced decay and significantly reduced the remaining mRNA amount down to ~13% (Fig. 5**F**). The faster decay rate is also reflected in a shorter TGFBR1 mRNA half-life of 9.48 h (95% CI: 8.23–10.91 h) in NANOS1 overexpressing cells compared to 18.12 h (95% CI: 15.23–21.78 h) in control cells.

From these data we concluded that NANOS1 is able to directly associate with the TGFBR1 mRNA leading to a destabilization of this transcript and thereby causing a reduced receptor expression. Consequently, we hypothesized that NANOS1 overexpressing cells should be less responsive to TGF-ß and its downstream signal transduction might be impaired. To test this hypothesis, we analyzed the protein expression of SMAD2 and SMAD3 as well as their TGF-ß-dependent phosphorylation. As expected, control cells showed a strong signaling response and increased the amount of p-SMAD2 and p-SMAD3 after TGF-ß stimulation. In contrast, NANOS1 overexpression efficiently prevented the phosphorylation of both SMADs after TGF-ß treatment without affecting the total amount of SMAD2/3 in a relevant manner (Fig. 5G). Since the phosphorylation of SMAD2 and SMAD3 triggers their translocation from the cytoplasm into the nucleus, we also analyzed the intracellular localization of both proteins in TGF-ß-treated control and NANOS1 overexpressing cells. Immunofluorescence staining allowed us to confirm the induced shuttling of SMAD2/3 in control cells after TGF-ß stimulation whereas NANOS1 overexpression strongly impaired this translocation (Fig. 5H).

In the nucleus, the SMAD complex associates with additional transcription factors in order to activate or repress TGF-ß target genes. Hence, we decided to investigate the transcriptional response of control and NANOS1 overexpressing cells using a SMAD3/4 binding element

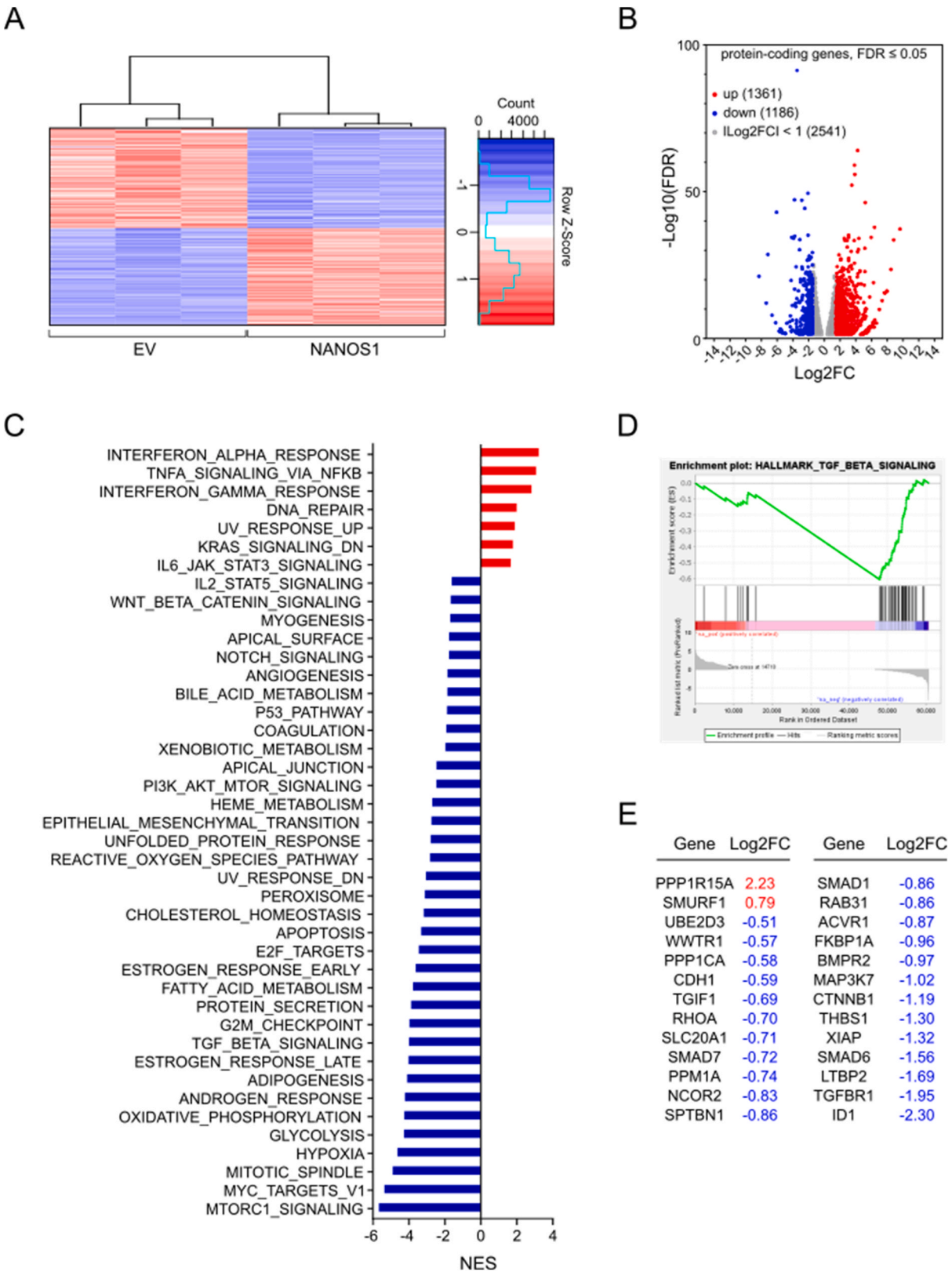

Gene	Log2FC	Gene	Log2FC
PPP1R15A	2.23	SMAD1	-0.86
SMURF1	0.79	RAB31	-0.86
UBE2D3	-0.51	ACVR1	-0.87
WWTR1	-0.57	FKBP1A	-0.96
PPP1CA	-0.58	BMPR2	-0.97
CDH1	-0.59	MAP3K7	-1.02
TGIF1	-0.69	CTNNB1	-1.19
RHOA	-0.70	THBS1	-1.30
SLC20A1	-0.71	XIAP	-1.32
SMAD7	-0.72	SMAD6	-1.56
PPM1A	-0.74	LTBP2	-1.69
NCOR2	-0.83	TGFBR1	-1.95
SPTBN1	-0.86	ID1	-2.30

Fig. 4. NANOS1 overexpression affects several pathways including TGF-ß signaling. A) Heatmap of significantly deregulated genes (FDR ≤ 0.05) after NANOS1 overexpression in SAS cells. B) Volcano plot of 5088 differentially expressed protein-coding genes with FDR ≤ 0.05. C) GSEA analysis of mRNA-sequencing data considering all protein-coding genes revealed a significant enrichment of seven as well as a reduction of 35 gene sets after NANOS1 overexpression. D) Enrichment plot depicting the depletion of TGF-ß signaling genes in NANOS1 overexpressing cells. E) List of significantly altered genes that belong to the HALLMARK_TGF_-BETA_SIGNALING gene set and their respective Log2FC values from mRNA-Seq.

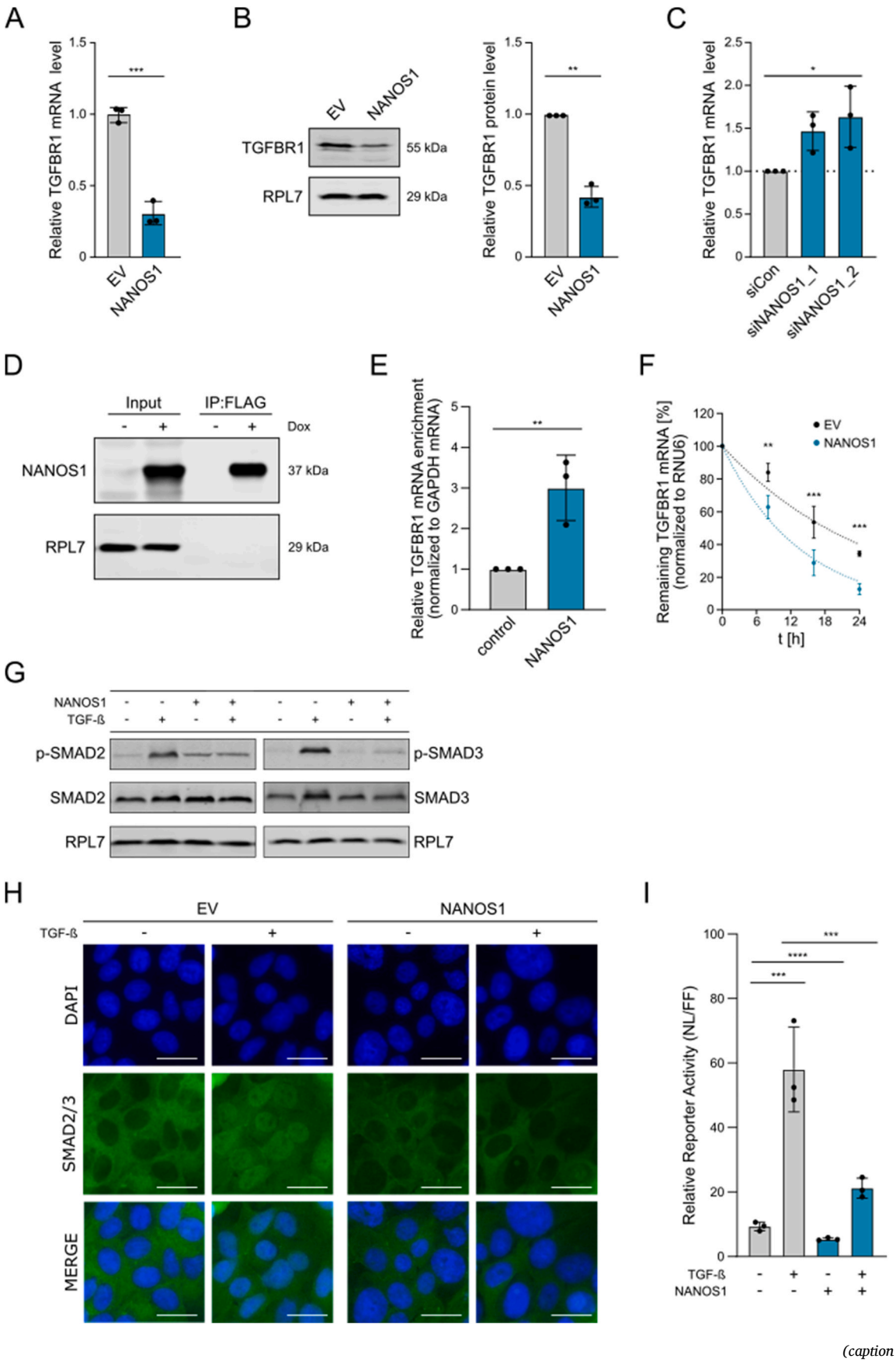

(caption on next page)

Fig. 5. NANOS1 regulates TGFBR1 expression and interferes with TGF-ß/SMAD signaling. A) Validation of NANOS1-dependent change in TGFBR1 mRNA abundance as measured by RT-qPCR. Normalization was performed using RPLP0 and PPIA. B) Representative western blot and the associated quantification of three independent biological replicates confirms decreased TGFBR1 protein expression upon NANOS1 overexpression in SAS cells. RPL7 served as loading control. C) TGFBR1 mRNA expression after NANOS1 knockdown in SAS cells. RT-qPCR was performed 72 h after siRNA transfection. D) Representative western blot analysis after anti-FLAG immunoprecipitation. SAS cells were treated with 1 µg/mL doxycycline (48 h) to induce expression of FLAG/HA-tagged NANOS1. Untreated cells did not express the tagged transgene and served as negative controls for subsequent RNA-Immunoprecipitation (RIP) assays. E) Analysis of co-purified TGFBR1 mRNA and its enrichment as determined by RT-qPCR after anti-FLAG immunoprecipitation showing a 3-fold higher binding of the TGFBR1 mRNA to NANOS1 as compared to GAPDH mRNA. All immunoprecipitation experiments were performed in biological replicates (n = 3). F) TGFBR1 mRNA stability analysis in SAS cells after alpha-amanitin treatment. EV and NANOS1 overexpressing cells were treated with the transcription inhibitor and harvested at the indicated time points. Expression levels were normalized to "0 h" and RNU6 was used as reference gene. Shown is the mean of three independent experiments (± standard deviation). Fitting curves were calculated using GraphPad Prism8 (one phase decay; $R^2 = 0.91$ (EV) and 0.96 (NANOS1), respectively). G) Analysis of TGF-ß/SMAD pathway activation upon TGF-ß stimulation in EV and NANOS1 overexpressing cells. Representative western blots from three independent replicates show TGF-ß-dependent phosphorylation of SMAD2 (S465/467) and SMAD3 (S423/425). RPL7 served as loading control. H) NANOS1 and EV control cells were treated for 48 h with 1 µg/mL Doxycycline and 10 ng/mL TGF-ß1 was added or not. Representative confocal images of three independent biological experiments show SMAD2/3 (green) expression and localization. Nuclei are stained with DAPI (blue). I) Smad-binding element (SBE) reporter assay was performed to measure downstream TGF-ß pathway activity under steady state conditions as well as after TGF-ß1 stimulation. Luminescence signal was measured in SAS EV and NANOS1 overexpressing cells transfected with NanoLuc (NL, reporter) and firefly luciferase (FF, control) and the ratio of NL/FF was calculated. High NL/FF ratio indicates high TGF-ß/SMAD pathway activation.

(SBE) luciferase reporter assay. We transfected EV control and NANOS1 overexpressing cells with the NanoLuc (NL) reporter plasmid as well as a plasmid encoding a firefly luciferase (FF) to control for transfection differences. After transfection, cells were treated with TGF-ß (or not) and the luciferase activities were measured. As expected, TGF-ß stimulation led to a ~6.2-fold increase of the NL activity reflective of a strong transcriptional response in control cells (Fig. 5I). Importantly, untreated NANOS1 overexpressing cells showed a significantly lower (~2-fold less) basal reporter activity compared to EV control cells. Furthermore, while the application of TGF-ß induced a transcriptional response also in NANOS1 overexpressing cells, this induction was significantly weaker and NL activity remained ~2.8-fold lower compared to EV control cells.

In conclusion, NANOS1 can bind to the TGFBR1 mRNA and decrease its stability leading to a reduced transcript and protein abundance. The reduced TGFBR1 level decreases the sensitivity of the cells towards TGF-ß and limits the transcriptional response thereby restricting the pro-tumorigenic effect of TGF-ß stimulation in NANOS1 overexpressing cells (Fig. 6).

4. Discussion

The metastatic progression of malignant tumors is a multifactorial phenomenon and our current understanding of the underlying molecular events as well as the relevant factors and their complex interplay is still limited. However, it is increasingly recognized that phenotypic plasticity, largely driven by non-genetic mechanisms, strongly influences the metastatic dissemination (LaFave et al., 2020; Marjanovic et al., 2020; Welch and Hurst, 2019). The EMT program, an important source of plasticity, enables transitions of malignant cells between different phenotypic states thereby enhancing motility and survival (Vig

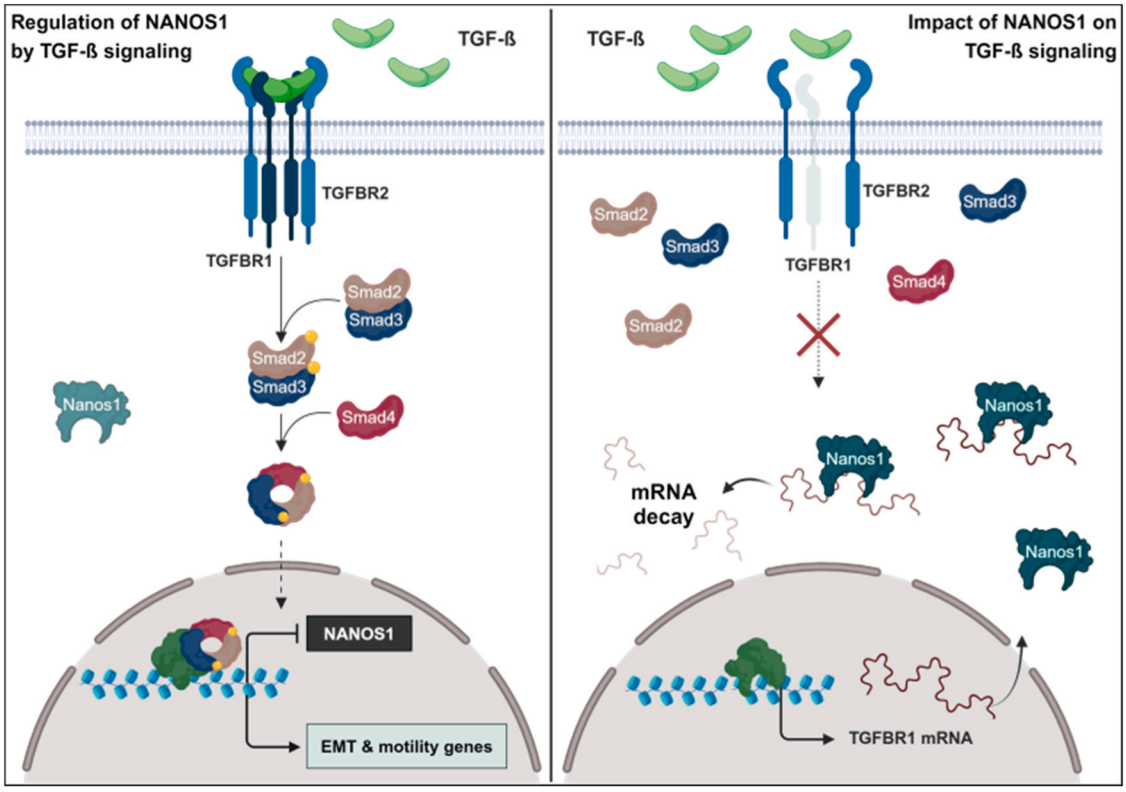

Fig. 6. Cross-regulation of NANOS1 and TGF-ß signaling. TGF-ß treatment decreases the expression of NANOS1 and increases cell motility through the induction of EMT. Oncogenic TGF-ß effects can be abrogated by the overexpression of NANOS1, which can bind to TGFBR1 mRNA leading to its enhanced decay and, consequently, a lower TGFBR1 protein abundance. Created with BioRender.com.

et al., 2015). EMT and its molecular mechanisms have been extensively studied and a crucial contribution of EMT to metastasis in oral cancer as well as several other cancer types has been described (Jayanthi et al., 2020; Lu and Kang, 2019). Of note, mounting evidence suggests that post-transcriptional events regulated by RBPs strongly contribute to the fine-tuning of EMT (Aparicio et al., 2013; Bebee et al., 2014). RBPs bind sequences or structural motifs within their target RNA. In this way they form ribonucleoprotein complexes and regulate important processes such as RNA splicing, polyadenylation, localization, translation, and RNA degradation. Consequently, RBPs are of great importance for maintaining cellular homeostasis and it is not surprising that several RBPs have been shown to be involved in a wide variety of human diseases including cancer making them promising therapeutic targets (Gerstberger et al., 2014; Bertoldo et al., 2023; Gebauer et al., 2021; He et al., 2023; Hentze et al., 2018; Weiße et al., 2020).

In this study we identified NANOS1 as a novel inhibitor of TGF-ß-induced EMT and cellular motility in human oral cancer cells. NANOS1 belongs to a highly conserved family of RBPs that comprises two additional members in humans, namely NANOS2 and NANOS3. NANOS proteins are best known for their crucial roles in germline development, although their contribution to cancer phenotypes is increasingly recognized (De Keuckelaere et al., 2018; Ilaslan et al., 2022). The first NANOS protein was originally discovered in *Drosophila melanogaster* where it was found to be essential for anterior–posterior axis polarity, abdomen formation, and germ cell development (Irish et al., 1989; Kobayashi et al., 1996; Wang and Lehmann, 1991). In order to fulfill this developmental function in the fruit fly, nanos forms a complex with pumilio and represses the expression of hunchback, an anterior morphogen. Pumilio recognizes specific sequence motifs that are present within the hunchback mRNA and upon binding it recruits nanos which triggers translational repression and degradation of the hunchback mRNA in the posterior (Sonoda and Wharton, 1999; Wharton and Struhl, 1991). This led to the idea that pumilio proteins confer specificity in RNA target selection while nanos acts as a cofactor for efficient repression. However, recent studies suggest that NANOS proteins can also directly bind to RNA and therefore might have PUMILIO-independent functions (Codino et al., 2021; Luo et al., 2020). Mechanistically, NANOS proteins contain a C-terminal zinc finger motif that is evolutionarily conserved between mammalian NANOS family members and those in lower organisms (Bhandari et al., 2014). This domain is crucial for NANOS function, as it facilitates binding to RNA and to other proteins like PUMILIO (Sonoda and Wharton, 1999; Jaruzelska et al., 2003). Moreover, all human NANOS proteins contain a conserved N-terminal NOT1 interacting motif (NIM) that enables interaction with the C-terminal domain of Negative regulator of transcription subunit 1 homolog (CNOT1), a component of the Carbon catabolite repressor protein 4 (CCR4)-NOT deadenylase complex (Bhandari et al., 2014). The CCR4–NOT complex is a highly conserved, multi-subunit complex that facilitates deadenylation and translational repression by recruiting additional proteins to the target RNA (Shirai et al., 2014). While the repressive function of NANOS proteins in the developmental context is well-established, their roles in human cancers are not well understood. In previous studies, NANOS1 was shown to be repressed by E-Cadherin in MDA-MB-231 breast cancer cells and its overexpression in DLD1 colon cancer cells did not alter total E-Cadherin expression, but interfered with the ability of the cells to form E-Cadherin-dependent three-dimensional aggregates. Consequently, NANOS1 overexpression could enhance DLD1 migration and invasion *in vitro* (Strumane et al., 2006). Furthermore, NANOS1 was shown to be higher expressed in more aggressive lung carcinomas and its overexpression in DLD1 cells increased, whereas its depletion in two breast cancer (Hs578T, BT549) as well as a lung cancer cell line (BZR) decreased Matrix Metallopeptidase 14 (MMP14) mRNA and protein expression and reduced the invasive properties of the breast and lung cancer cells (Bonnomet et al., 2008). However, it remains unclear how NANOS1 is able to regulate E-Cadherin function and MMP14 expression. We note here that MMP14 mRNA expression is significantly decreased in SAS cells overexpressing NANOS1 (see Supplementary Data 2), which is opposite to what has been described previously. Moreover, E-Cadherin and NANOS1 are both downregulated in SAS cells upon TGF-ß treatment whereas the overexpression of NANOS1 slightly decreases E-Cadherin mRNA expression levels (see Supplementary Data 1 and 2), which is again not consistent with previous observations. These findings suggest that NANOS1 might have tissue and/or cancer type-specific oncogenic or tumor suppressive functions. In fact, Ilaslan *et al.* analyzed publicly available expression datasets of cancer and normal tissues and found that NANOS1 is overexpressed in brain, kidney, liver, lung, ovary, pancreas, skin, thyroid gland, uterus, and testis cancers. On the other hand, NANOS1 expression is diminished in bladder, colon, oesophagus, and stomach cancers (Ilaslan et al., 2022). Of note, the observed downregulation of NANOS1 in colon cancer and the unaltered expression in breast cancer is rather unexpected given the published pro-oncogenic functions in these cancer types (Bonnomet et al., 2008; Strumane et al., 2006). Importantly, our functional data presented herein show that NANOS1 can decrease the motility of oral cancer cells and act as a negative post-transcriptional regulator of oncogenic TGF-ß signaling by reducing the expression of TGFBR1 suggesting that NANOS1 can indeed also act as a tumor suppressor. This is further supported by clinical data that show a correlation between NANOS1 mRNA expression and patient survival. In detail, we found that low expression of NANOS1 is significantly correlated with a poor overall survival in oral cancers that originated in the tongue, and low NANOS1 expression in the classical subtype of HNSCC is also correlated with a worse disease free survival (Suppl. Fig. 3). Hence, in the majority of human cancers the contribution of NANOS1 to carcinogenesis remains unknown. Therefore, much more experimental work is required, which also includes the generation of knockout and transgenic mouse models, which are currently not available, to study the role of NANOS1 in different cancer models. Along these lines, we performed additional preliminary studies. In order to test if NANOS1 is able to inhibit cell motility in other non-glandular epithelial cell lines, we analyzed the regulation of NANOS1 by TGF-ß and its impact on cell motility in A-375 melanoma cells. Intriguingly, we observed a downregulation of NANOS1 upon TGF-ß stimulation (Suppl. Fig. 4A). Moreover, transgenic overexpression of NANOS1 in A-375 cells had an inhibitory effect on cell proliferation, 2D-migration as well as trans-migration and trans-invasion (Suppl. Fig. 4B–F). Analyses of publically available TCGA data from skin cutaneous melanoma (SKCM) using GEPIA2 revealed that low NANOS1 expression significantly correlated with poor overall as well as disease free survival (Suppl. Fig. 4G). These additional findings will lay the foundation for future mechanistic studies that will focus on the identification of NANOS1 target transcripts that are bound by NANOS1 in a PUMILIO-dependent or independent manner. This will be important to understand direct and indirect effects of NANOS1 on the cancer transcriptome. Importantly, our current data suggest for the first time that NANOS1 can directly regulate the expression of TGFBR1 and thus restrict the oncogenic effects of TGF-ß signaling in oral cancer cells. Recent studies identified additional RBPs that regulate TGFBR1 expression post-transcriptionally. For example, Wang et al. identified Quaking 5 (QKI-5) as an inhibitor of TGF-ß-induced EMT and invasion in lung cancer by decreasing the stability of the TGFBR1 mRNA which is similar to our herein proposed mechanism of action of NANOS1 (Wang et al., 2021). In contrast, Zhu and colleagues identified the long non-coding RNA LINC01232 that promotes TGFBR1 mRNA stability in human lung cancer cells via recruiting Insulin-like growth factor 2 mRNA-binding protein 2 (IGF2BP2) (Zhu et al., 2022). This stabilizing effect of Igf2bp2 was also observed recently in murine hepatic stellate cells which also upregulated Igf2bp2 expression upon TGF-ß stimulation (Xu et al., 2022). These and other findings suggest an intimate link between TGF-ß signaling and RBPs. Hence, it will be interesting to understand how different RBPs act in concert to affect the fate of an individual target RNA. Furthermore, conserved as well as cell

type-specific post-transcriptional regulators of TGF-ß pathway components should be identified in order to broaden our understanding of the context-dependency of TGF-ß signaling (David and Massague, 2018; Morikawa et al., 2016). Of note, the regulation of NANOS1 by TGF-ß seems to be conserved and can also be seen in normal murine mammary gland (NMuMG) cells (Meyer-Schaller et al., 2019). Hence, future studies should investigate the underlying mechanisms that are responsible for the downregulation of NANOS1 during TGF-ß-induced EMT. Importantly, interfering with this repression might have therapeutic relevance and could limit the metastatic spread of cancer cells.

Funding source

This study was supported by intramural funding from the Medical Faculty to TG.

CRediT authorship contribution statement

Roland Jacob: Formal analysis, Methodology. **Jonas Pyko:** Formal analysis, Methodology, Visualization. **Jana Macho:** Investigation, Validation. **Tony Gutschner:** Conceptualization, Formal analysis, Funding acquisition, Methodology, Project administration, Resources, Supervision, Visualization, Writing – original draft, Writing – review & editing. **Monika Haemmerle:** Conceptualization, Writing – original draft, Writing – review & editing. **Alexander W. Eckert:** Resources. **Matthias Kappler:** Resources. **Julia Rosemann:** Conceptualization, Data curation, Formal analysis, Investigation, Methodology, Project administration, Visualization, Writing – original draft, Writing – review & editing.

Declaration of Competing Interest

The authors declare that they have no known competing financial interests or personal relationships that could have appeared to influence the work reported in this paper.

Data Availability

Data will be made available on request.

Acknowledgments

The authors would like to thank all members of the Gutschner & Hämmerle labs for helpful discussions as well as the Core Facility Imaging (CFI) and Dr. Nadine Bley for help with IncuCyte measurements and Drs. Markus Glaß and Danny Misiak for RNA-Seq analyses.

Appendix A. Supporting information

Supplementary data associated with this article can be found in the online version at doi:10.1016/j.ejcb.2024.151400.

References

Aparicio, L.A., et al., 2013. Posttranscriptional regulation by RNA-binding proteins during epithelial-to-mesenchymal transition. Cell Mol. Life Sci. 70 (23), 4463–4477.
Baraniak, A.P., Chen, J.R., Garcia-Blanco, M.A., 2006. Fox-2 mediates epithelial cell-specific fibroblast growth factor receptor 2 exon choice. Mol. Cell Biol. 26 (4), 1209–1222.
Bebee, T.W., Cieply, B.W., Carstens, R.P., 2014. Genome-wide activities of RNA binding proteins that regulate cellular changes in the epithelial to mesenchymal transition (EMT). Adv. Exp. Med Biol. 825, 267–302.
Bertoldo, J.B., Muller, S., Huttelmaier, S., 2023. RNA-binding proteins in cancer drug discovery. Drug Discov. Today 28 (6), 103580.
Bhandari, D., et al., 2014. Structural basis for the Nanos-mediated recruitment of the CCR4-NOT complex and translational repression. Genes Dev. 28 (8), 888–901.
Bonnomet, A., et al., 2008. The E-cadherin-repressed hNanos1 gene induces tumor cell invasion by upregulating MT1-MMP expression. Oncogene 27 (26), 3692–3699.
Bonomi, S., et al., 2013. HnRNP A1 controls a splicing regulatory circuit promoting mesenchymal-to-epithelial transition. Nucleic Acids Res. 41 (18), 8665–8679.
Brabletz, T., et al., 2018. EMT in cancer. Nat. Rev. Cancer 18 (2), 128–134.
Braeutigam, C., et al., 2014. The RNA-binding protein Rbfox2: an essential regulator of EMT-driven alternative splicing and a mediator of cellular invasion. Oncogene 33 (9), 1082–1092.
Chaudhury, A., et al., 2010. TGF-beta-mediated phosphorylation of hnRNP E1 induces EMT via transcript-selective translational induction of Dab2 and ILEI. Nat. Cell Biol. 12 (3), 286–293.
Codino, A., et al., 2021. NANOS2 is a sequence-specific mRNA-binding protein that promotes transcript degradation in spermatogonial stem cells. iScience 24 (7), 102762.
David, C.J., Massague, J., 2018. Contextual determinants of TGFbeta action in development, immunity and cancer. Nat. Rev. Mol. Cell Biol. 19 (7), 419–435.
De Keuckelaere, E., et al., 2018. Nanos genes and their role in development and beyond. Cell Mol. Life Sci. 75 (11), 1929–1946.
Dorn, A., et al., 2020. LINC00261 IS Differentially Expressed In Pancreatic Cancer Subtypes And Regulates a pro-epithelial cell identity. Cancers 12 (5).
Gebauer, F., et al., 2021. RNA-binding proteins in human genetic disease. Nat. Rev. Genet 22 (3), 185–198.
Gerstberger, S., Hafner, M., Tuschl, T., 2014. A census of human RNA-binding proteins. Nat. Rev. Genet. 15 (12), 829–845.
He, S., et al., 2023. The nexus between RNA-binding proteins and their effectors. Nat. Rev. Genet. 24 (5), 276–294.
Heldin, C.H., Vanlandewijck, M., Moustakas, A., 2012. Regulation of EMT by TGFbeta in cancer. FEBS Lett. 586 (14), 1959–1970.
Hentze, M.W., et al., 2018. A brave new world of RNA-binding proteins. Nat. Rev. Mol. Cell Biol. 19 (5), 327–341.
Horiguchi, K., et al., 2012. TGF-beta drives epithelial-mesenchymal transition through deltaEF1-mediated downregulation of ESRP. Oncogene 31 (26), 3190–3201.
Howley, B.V., Howe, P.H., 2019. TGF-beta signaling in cancer: post-transcriptional regulation of EMT via hnRNP E1. Cytokine 118, 19–26.
Hussey, G.S., et al., 2011. Identification of an mRNP complex regulating tumorigenesis at the translational elongation step. Mol. Cell 41 (4), 419–431.
Ilaslan, E., et al., 2022. Emerging roles of NANOS RNA-binding proteins in Cancer. Int. J. Mol. Sci. 23 (16).
Irish, V., Lehmann, R., Akam, M., 1989. The Drosophila posterior-group gene nanos functions by repressing hunchback activity. Nature 338 (6217), 646–648.
Janakiraman, H., et al., 2018. The long (lncRNA) and short (miRNA) of It: TGFbeta-mediated control of RNA-binding proteins and noncoding RNAs. Mol. Cancer Res. 16 (4), 567–579.
Jaruzelska, J., et al., 2003. Conservation of a Pumilio-Nanos complex from Drosophila germ plasm to human germ cells. Dev. Genes Evol. 213 (3), 120–126.
Jayanthi, P., Varun, B.R., Selvaraj, J., 2020. Epithelial-mesenchymal transition in oral squamous cell carcinoma: an insight into molecular mechanisms and clinical implications. J. Oral. Maxillofac. Pathol. 24 (1), 189.
Jbara, A., et al., 2023. RBFOX2 modulates a metastatic signature of alternative splicing in pancreatic cancer. Nature 617 (7959), 147–153.
Kalluri, R., Weinberg, R.A., 2009. The basics of epithelial-mesenchymal transition. J. Clin. Investig. 119 (6), 1420–1428.
Kobayashi, S., et al., 1996. Essential role of the posterior morphogen nanos for germline development in Drosophila. Nature 380 (6576), 708–711.
LaFave, L.M., et al., 2020. Epigenomic state transitions characterize tumor progression in mouse lung adenocarcinoma. Cancer Cell 38 (2), p. 212-228 e13.
Lamouille, S., Xu, J., Derynck, R., 2014. Molecular mechanisms of epithelial-mesenchymal transition. Nat. Rev. Mol. Cell Biol. 15 (3), 178–196.
Lu, W., Kang, Y., 2019. Epithelial-mesenchymal plasticity in Cancer progression and metastasis. Dev. Cell 49 (3), 361–374.
Luo, E.C., et al., 2020. Large-scale tethered function assays identify factors that regulate mRNA stability and translation. Nat. Struct. Mol. Biol. 27 (10), 989–1000.
Marjanovic, N.D., et al., 2020. Emergence of a high-plasticity cell state during lung Cancer evolution. Cancer Cell 38 (2), p. 229-246 e13.
Meyer-Schaller, N., et al., 2019. A hierarchical regulatory landscape during the multiple stages of EMT. Dev. Cell 48 (4), p. 539-553 e6.
Mootha, V.K., et al., 2003. PGC-1alpha-responsive genes involved in oxidative phosphorylation are coordinately downregulated in human diabetes. Nat. Genet. 34 (3), 267–273.
Morikawa, M., Derynck, R., Miyazono, K., 2016. TGF-beta and the TGF-beta family: context-dependent roles in cell and tissue physiology. Cold Spring Harb. Perspect. Biol. 8 (5).
Oshimori, N., Oristian, D., Fuchs, E., 2015. TGF-beta promotes heterogeneity and drug resistance in squamous cell carcinoma. Cell 160 (5), 963–976.
Pickup, M., Novitskiy, S., Moses, H.L., 2013. The roles of TGFbeta in the tumour microenvironment. Nat. Rev. Cancer 13 (11), 788–799.
Principe, D.R., et al., 2014. TGF-beta: duality of function between tumor prevention and carcinogenesis. J. Natl. Cancer Inst. 106 (2), djt369.
Schindelin, J., et al., 2012. Fiji: an open-source platform for biological-image analysis. Nat. Methods 9 (7), 676–682.
Schneider, C.A., Rasband, W.S., Eliceiri, K.W., 2012. NIH Image to ImageJ: 25 years of image analysis. Nat. Methods 9 (7), 671–675.
Shirai, Y.T., et al., 2014. Multifunctional roles of the mammalian CCR4-NOT complex in physiological phenomena. Front. Genet. 5, 286.
Sonoda, J., Wharton, R.P., 1999. Recruitment of Nanos to hunchback mRNA by Pumilio. Genes Dev. 13 (20), 2704–2712.

Strumane, K., et al., 2006. E-cadherin regulates human Nanos1, which interacts with p120ctn and induces tumor cell migration and invasion. Cancer Res. 66 (20), 10007–10015.
Subramanian, A., et al., 2005. Gene set enrichment analysis: a knowledge-based approach for interpreting genome-wide expression profiles. Proc. Natl. Acad. Sci. 102 (43), 15545–15550.
Tang, Z., et al., 2019. GEPIA2: an enhanced web server for large-scale expression profiling and interactive analysis. Nucleic Acids Res. 47 (W1), W556–W560.
Tripathi, V., et al., 2016. Direct regulation of alternative splicing by SMAD3 through PCBP1 is essential to the tumor-promoting role of TGF-beta. Mol. Cell 64 (3), 549–564.
Venables, J.P., et al., 2013. RBFOX2 is an important regulator of mesenchymal tissue-specific splicing in both normal and cancer tissues. Mol. Cell Biol. 33 (2), 396–405.
Vig, N., Mackenzie, I.C., Biddle, A., 2015. Phenotypic plasticity and epithelial-to-mesenchymal transition in the behaviour and therapeutic response of oral squamous cell carcinoma. J. Oral. Pathol. Med. 44 (9), 649–655.
Wang, C., Lehmann, R., 1991. Nanos is the localized posterior determinant in Drosophila. Cell 66 (4), 637–647.
Wang, H., et al., 2010. PCBP1 suppresses the translation of metastasis-associated PRL-3 phosphatase. Cancer Cell 18 (1), 52–62.
Wang, S., et al., 2021. Quaking 5 suppresses TGF-beta-induced EMT and cell invasion in lung adenocarcinoma. EMBO Rep. 22 (6), e52079.
Wang, T., et al., 2014. Genetic screens in human cells using the CRISPR-Cas9 system. Science 343 (6166), 80–84.
Warzecha, C.C., et al., 2010. An ESRP-regulated splicing programme is abrogated during the epithelial-mesenchymal transition. Embo J. 29 (19), 3286–3300.
Weiße, J., et al., 2020. RNA-binding proteins as regulators of migration, invasion and metastasis in oral squamous cell carcinoma. Int. J. Mol. Sci. 21 (18).
Weiße, J., et al., 2021. Identification of lymphocyte cell-specific protein-tyrosine kinase (LCK) as a driver for invasion and migration of oral cancer by tumor heterogeneity exploitation. Mol. Cancer 20 (1), 88.
Welch, D.R., Hurst, D.R., 2019. Defining the hallmarks of metastasis. Cancer Res. 79 (12), 3011–3027.
Wharton, R.P., Struhl, G., 1991. RNA regulatory elements mediate control of Drosophila body pattern by the posterior morphogen nanos. Cell 67 (5), 955–967.
Xu, Y., et al., 2014. Cell type-restricted activity of hnRNPM promotes breast cancer metastasis via regulating alternative splicing. Genes Dev. 28 (11), 1191–1203.
Xu, Z., et al., 2022. Igf2bp2 knockdown improves CCl(4)-induced liver fibrosis and TGF-beta-activated mouse hepatic stellate cells by regulating Tgfbr1. Int. Immunopharmacol. 110, 108987.
Zhang, M., et al., 2016. Poly r(C) binding protein (PCBP) 1 is a negative regulator of thyroid carcinoma. Am. J. Transl. Res. 8 (8), 3567–3573.
Zhang, Z.Z., et al., 2015. HOTAIR long noncoding RNA promotes gastric Cancer metastasis through suppression of poly r(C)-binding protein (PCBP) 1. Mol. Cancer Ther. 14 (5), 1162–1170.
Zhou, Z.J., et al., 2014. HNRNPAB induces epithelial-mesenchymal transition and promotes metastasis of hepatocellular carcinoma by transcriptionally activating SNAIL. Cancer Res. 74 (10), 2750–2762.
Zhu, L., et al., 2022. FOXP3 activated-LINC01232 accelerates the stemness of non-small cell lung carcinoma by activating TGF-beta signaling pathway and recruiting IGF2BP2 to stabilize TGFBR1. Exp. Cell Res. 413 (2), 113024.